

# AN EIGENSTRUCTURE APPROACH FOR THE RETRIEVAL OF CYLINDRICAL HARMONICS

Ahmed H. Tewfik      Bernard C. Levy  
Alan S. Willsky

Laboratory for Information and Decision Systems and  
The Department of Electrical Engineering and Computer Science  
Massachusetts Institute of Technology, Cambridge, MA 02139

October 8, 1986

## Abstract

In this paper, we present a high resolution spectral estimation method for 2-D isotropic random fields with covariance functions equal to weighted sums of cylindrical harmonics. Such fields are often used to model some types of background noises in geophysics and in ocean acoustics. The approach that we present differs from previous 2-D spectral estimation techniques by the fact that we take maximal advantage of the symmetries implied by both the isotropy and the special covariance structure of these fields. Note that isotropy is the natural generalization to several dimensions of the 1-D notion of stationarity. Our approach is similar in spirit to 1-D harmonic retrieval techniques, such as the MUSIC method, which rely on an eigenanalysis of the covariance matrix. In the 2-D isotropic context, we begin with a Fourier series representation of an isotropic field with respect to the angle  $\theta$  in a polar coordinate representation of the underlying 2-D space. We then obtain a spectral estimate by performing an eigenanalysis of the covariance matrix of samples of the zeroth-order Fourier coefficient process in order to extract the cylindrical harmonics. We also discuss the estimation of this covariance matrix and present examples to illustrate the high resolution and robustness properties of our procedure.

---

\*This work was supported by the National Science Foundation under Grant No. ECS-83-12921 and by the Army Research Office under Grant No. DAAG-84-K-0005.

# 1 INTRODUCTION

Array processing is a popular technique for solving estimation problems involving propagating waves. For example, in geophysical applications, arrays of sensors are often used to discriminate between earthquakes and underground nuclear explosions. In sonar, an array of receiving hydrophones may provide data for determining the spatial coordinates of underwater targets. Arrays of receivers often work against a background noise field. Knowledge of the frequency-wave-number power spectrum of the background noise field is important for studying the performance of optimal array processing schemes [1]. Several multidimensional spectral estimation methods have been developed in the past and can be used to estimate the frequency-wave-number power spectrum of the background noise impinging on any given array of sensors. (See [2] for a good review of multidimensional spectral estimators and [3] for the application of some spectral estimation methods to array processing problems.) These methods are very general and do not attempt to exploit any special structure of the power spectrum to be estimated.

In this paper, by contrast, we present a new high resolution spectral estimation method for a class of 2-D *isotropic* random fields that is often used to model some types of background noises in both geophysics and ocean acoustics. Our algorithm uses the special structure of the covariance function of the isotropic random fields in this class. Isotropic fields are characterized by the fact that their mean value is a constant independent of position and their autocovariance function is invariant under all rigid body motions, i.e. under translations and rotations. In some sense, isotropy is the natural extension of the notion of stationarity in one dimension.

The specific class of 2-D isotropic fields that we consider corresponds to fields whose covariance function can be modeled as a weighted sum of *cylindrical harmonics*. The term cylindrical harmonics is used in this context to denote a radially symmetric function  $f(\vec{r})$ <sup>1</sup>, of the form  $J_0(\lambda_k r)$  where  $\lambda_k$  is a fixed two-dimensional “cylindrical frequency” measured in radians

---

<sup>1</sup>Throughout this paper we use  $\vec{r}$  to denote a point in 2-D Cartesian space. The polar coordinates of this point are denoted by  $r$  and  $\theta$ .

per unit distance. Such covariance functions arise in geophysics whenever the background noise field consists of either fundamental-mode, or higher mode, Rayleigh waves propagating uniformly from all azimuths simultaneously [1]. The covariance function of the “circle noise” [4] in ocean acoustics is also of this particular form. Note that the two-dimensional Fourier transform of a cylindrical harmonic is radially symmetric in the wave-number plane and consists of a *cylindrical* impulse at a radial frequency of  $\lambda_k$  radians per unit distance (i.e. the Fourier transform is a 1-D sheet of impulses concentrated on a circle of radius  $\lambda_k$ ). Hence, our problem is to determine the number, location and amplitude of the cylindrical impulses in the wave-number spectrum of an isotropic field. This problem differs from the one which was investigated by Lang and McClellan [5] and by Wax and Kailath [6], who extended Pisarenko’s method [7] and the MUSIC method [8],[9] respectively, and used them to estimate power spectra which are equal to a weighted sum of multidimensional *point* impulses.

This paper is organized as follows. In Section 2 we make clear the central role of the Fourier series representation of isotropic fields with respect to the angle  $\theta$  in a polar coordinate representation of the underlying 2-D space. We also demonstrate that the covariance function of the full process can be recovered from that of its zeroth-order Fourier coefficient process, i.e. the process obtained by averaging the random field on circles centered at the origin. Following some motivation for considering the class of isotropic covariance functions that are equal to a weighted sum of cylindrical harmonics, we formulate the problem of retrieving cylindrical harmonics from the covariance of samples of the zeroth-order Fourier coefficient process. Then, in Section 3 we present a new algorithm for recovering such covariances by performing an eigenanalysis of the covariance matrix of samples of the zeroth order Fourier coefficient process corresponding to the measurements. Both the theory behind this algorithm and its numerical implementation are discussed. The proposed algorithm is very similar in spirit to the eigenstructure approach developed by Schmidt [8], and by Bienvenu and Kopp [9] for solving the 1-D harmonic retrieval problem. Section 4 presents a method for estimating the covariance matrix that is used as an input to

our procedure. Both the statistical properties of the covariance estimate and its practical implementation are presented. In particular, our estimate is shown to be both unbiased and consistent, and an example is provided to demonstrate this fact. Finally, two examples are presented in Section 5 to illustrate the high resolution and robustness properties of our method.

## 2 CYLINDRICAL HARMONICS RETRIEVAL PROBLEM

We begin this section by reviewing some of the properties of isotropic random fields. In particular, we focus our attention on Fourier series representations of such fields with respect to the angle  $\theta$  in a polar coordinate representation of the underlying 2-D space.

### A Fourier Series for Isotropic Random Fields

The covariance function

$$K(\vec{r}) = E[z(\vec{v})z(\vec{v} + \vec{r})] \quad (2.1)$$

of any zero-mean isotropic random field  $z(\vec{r})$  is a function of  $r$  only, so that, by abuse of notation we can write

$$K(\vec{r}) = K(r). \quad (2.2)$$

Such a field can be expanded into a Fourier series of the form [10]

$$z(\vec{r}) = \sum_{n=-\infty}^{\infty} z_n(r) e^{jn\theta}, \quad (2.3)$$

$$z_n(r) = \frac{1}{2\pi} \int_0^{2\pi} z(\vec{r}) e^{-jn\theta} d\theta, \quad (2.4)$$

where the Fourier coefficient processes of different orders are uncorrelated, i.e.

$$E[z_n(r)z_m(s)] = 0, \quad (2.5)$$

for  $n \neq m$ . The covariance function  $k_n(r, s)$  of the  $n$ th order Fourier coefficient  $z_n(r)$  is given by [10]

$$\begin{aligned} k_n(r, s) &= E[z_n(r)z_n(s)] \\ &= \frac{1}{2\pi} \int_0^{2\pi} J_n(\lambda r) J_n(\lambda s) S(\lambda) \lambda d\lambda. \end{aligned} \quad (2.6)$$

In (2.6)  $J_n(\cdot)$  is the Bessel function of order  $n$  and  $S(\lambda)$  is the power spectrum associated with  $z(\vec{r})$ , i.e.

$$\begin{aligned} S(\vec{\lambda}) &= \int_{\mathbf{R}^2} K(\vec{r}) e^{-j\vec{\lambda}\cdot\vec{r}} d\vec{r} \\ &= 2\pi \int_0^\infty K(r) J_0(\lambda r) r dr \\ &= S(\lambda), \end{aligned} \tag{2.7}$$

where  $\lambda = |\vec{\lambda}|$  is the magnitude of the wave vector  $\vec{\lambda}$ , and where we have taken advantage of the circular symmetry of  $K(\vec{r})$ . By using the addition theorem for Bessel functions [11], it can also be shown that  $k_n(r, s)$  can be computed from  $K(r)$  as

$$k_n(r, s) = \frac{1}{2\pi} \int_0^{2\pi} K((r^2 + s^2 - 2rs \cos \theta)^{1/2}) e^{-jn\theta} d\theta. \tag{2.8}$$

Let us now make two comments. The first is that although  $z(\vec{r})$  is isotropic,  $z_n(r)$  is *not* a stationary process, i.e.  $k_n(r, s)$  is *not* a function of  $r - s$ . Secondly, both the covariance function  $K(r)$  of the full process  $z(\vec{r})$  and its power spectrum  $S(\lambda)$  can be recovered exactly from  $k_0(r, s)$  as follows. By specializing (2.8) to the case  $n = 0$  we obtain for  $s = 0$

$$K(r) = k_0(r, 0). \tag{2.9}$$

Furthermore,  $S(\lambda)$  can be recovered from  $k_n(r, s)$  in general by observing that (2.6) implies that the  $n$ th order Hankel transform [12] of  $k_n(r, s)$  with respect to the variable  $r$  is just  $S(\lambda) J_n(\lambda s) / 2\pi$ . Hence, given  $k_n(r, s)$ ,  $S(\lambda)$  can be computed as

$$S(\lambda) = 2\pi \int_0^\infty J_n(\lambda r) k_n(r, s) r dr / J_n(\lambda s). \tag{2.10}$$

Thus, if we are interested in extracting information from  $K(r)$ , or from its associated power spectrum  $S(\lambda)$ , we can as well focus our attention on the covariance  $k_0(r, s)$  without any loss of information. This important observation is the key to the high resolution spectral estimation procedure that we shall present in the next section.

## B Motivation and Problem Statement

As mentioned earlier, array processing is a popular technique for solving estimation problems involving propagating waves. Such problems arise in geophysics and in ocean acoustics, among other fields. Arrays of receivers often work against a background noise field. Knowledge of the frequency-wave-number power spectrum of the background noise field is important for studying the performance of optimal array processing schemes [1]. In many applications, the medium in which the waves of interest are propagating supports surface waves; for example Rayleigh and Love waves or internal ocean waves. In such applications, the background noise is often modeled as consisting of a large number of independent waves propagating from all azimuths simultaneously with the same velocity  $c$  m/sec and with the same frequency  $f_0$  Hertz. The frequency-wave-number power spectrum of such a background noise has the form [1],[4]

$$S(\omega : \vec{\lambda}) = 2\pi C \frac{\delta(\lambda - \lambda_0)}{\lambda}, \quad (2.11)$$

where  $C$  is a positive constant and where  $\lambda_0 = 2\pi f_0/c$  is the wave-number of the background noise in rad/m. A background noise that has a frequency-wave-number power spectrum of the form (2.11) is called a *circle noise* in [4] and has a temporal frequency spatial correlation function (i.e. the inverse Fourier transform of  $S(\omega : \vec{\lambda})$  with respect to  $\vec{\lambda}$ ) of the form

$$K(\omega : \vec{r}) = C J_0(\lambda_0 r). \quad (2.12)$$

Observe that  $K(\omega : \vec{r})$  is a cylindrical harmonic. In some situations, the background noise can be a superposition of a number  $L$  of circle noises of different wave-numbers, and one is then interested in estimating both the cylindrical frequencies corresponding to the circle noise wave-numbers  $\lambda_l$  and the cylindrical harmonics amplitudes  $C_l$  for  $1 \leq l \leq L$ , in order for example to evaluate the performance of any processing array which is to be used in the presence of such a background noise field.

In other situations, one might be interested in finding the propagating surface modes that an isotropic medium of interest can support. In this case, one can excite the medium with a large number of independent wide-band directional sources uniformly distributed over the circumference of a

circle whose radius is large compared to any wavelength of interest, and all radiating towards the center of the circle. One then measures the response of the medium close to the center of such a circle. If the isotropic medium can support only a finite number of wave-numbers then the resulting waves will have a frequency-wave-number power spectrum of the form (2.11).

In all of the above situations, there is a need to estimate isotropic covariance functions that are equal to a weighted sum of cylindrical harmonics. This is the problem that we consider in this paper. We shall assume that we are given some noisy measurements  $y(\vec{r})$  of a Gaussian isotropic random field  $z(\vec{r})$  whose covariance function is of the form

$$K(r) = \sum_{l=1}^L P_l J_0(\lambda_l r), \quad (2.13)$$

or equivalently whose power spectrum is of the form

$$S(\lambda) = \sum_{l=1}^L P_l \frac{\delta(\lambda - \lambda_l)}{\lambda}. \quad (2.14)$$

Specifically, we assume that measurements  $y(\vec{r})$  are made on a finite set of concentric circles of radii  $\{r_i : 1 \leq i \leq I\}$ , and that  $y(r_i, \theta)$  is given by

$$y(r_i, \theta) = z(r_i, \theta) + n(r_i, \theta), \quad 0 \leq \theta \leq 2\pi. \quad (2.15)$$

In (2.15) the observation noise  $n(r_i, \theta)$  is uncorrelated with  $z(\vec{r})$  and is a zero-mean Gaussian white noise process of intensity  $\sigma^2$  in the discrete radial coordinate  $r_i$  and the continuous angle coordinate  $\theta$ , i.e.

$$E[n(r_i, \theta)] = 0, \quad (2.16)$$

$$E[n(r_i, \theta)n(r_j, \phi)] = \sigma^2 \frac{\delta_{i,j}}{r_i} \delta(\theta - \phi). \quad (2.17)$$

Our objective is to solve the cylindrical harmonics retrieval problem, i.e. to simultaneously estimate the measurement noise power  $\sigma^2$  and to reconstruct  $S(\lambda)$  by finding the cylindrical harmonics powers  $P_l$  and the cylindrical harmonics frequencies  $\lambda_l$ .

Note the parallel between the cylindrical harmonics retrieval problem that we have described above and the 1-D harmonic retrieval problem where

one is interested in estimating a *stationary* covariance function that is equal to a weighted sum of exponential functions. In the 1-D case, the objective is to estimate both the location and amplitude of a number of 1-D impulses in the frequency domain while in the 2-D case the goal is to find the location and amplitude of a number of cylindrical impulses in the wave-number plane. It will turn out that the algorithm that we propose in the next section for solving the cylindrical harmonics retrieval problem is very similar in spirit to 1-D harmonic retrieval procedures [8], [9] based on an eigenanalysis of a covariance matrix, even though our algorithm uses samples of the *non-stationary* covariance function of the zeroth-order Fourier coefficient process corresponding to the measurements  $y(\vec{r})$ .

Finally, observe that the harmonic retrieval problem can be solved by using any of the high resolution 2-D spectral estimation methods. As mentioned earlier, these methods are very general and do not exploit any special property of the power spectrum to be estimated. By comparison, our procedure takes explicitly into account the isotropy property of  $y(\vec{r})$ , as well as the special structure (2.14) of the spectrum that we want to estimate.

### 3 THE EIGENSTRUCTURE APPROACH

In one-dimensional signal processing, several eigenstructure methods have been proposed to solve the 1-D harmonic retrieval problem, i.e. the problem of estimating covariance functions of the form

$$r(i, j) = \sigma^2 \delta_{i,j} + \sum_{l=1}^L P_l \cos(2\pi f_l(i-j)\Delta t), \quad (3.1)$$

where  $\delta_{i,j}$  is a Kronecker delta. These techniques require an eigenanalysis of the autocorrelation matrix  $R = [r(i, j)]$ . In particular, Pisarenko's method [7] uses the value of the smallest eigenvalue of  $R$  as an estimate of the noise power  $\sigma^2$ . The locations of the frequencies  $f_l$  are then determined by finding the zeros of a polynomial whose coefficients are the elements of the eigenvector corresponding to the smallest eigenvalue. The disadvantage of this method lies in the fact that, as the size of the matrix  $R$  grows, (a necessary feature for resolving closely spaced frequencies), the number of close eigenvalues corresponding to the white noise component of the signal becomes large, leading to an ill-conditioned eigenvector determination problem [13]. To overcome this problem, Schmidt [8] and Bienvenu and Kopp [9] noted that the computation of the subspace spanned by the eigenvectors corresponding to the set of smallest eigenvalues is much less sensitive to perturbations in the entries of the matrix  $R$ , than the computation of individual eigenvectors. The methods they proposed use the whole eigenspace associated with the cluster of smallest eigenvalues to estimate the frequencies of model (3.1). In this section, we shall develop an algorithm for solving the cylindrical harmonics retrieval problem which is very similar in spirit to those of Schmidt and Bienvenu and Kopp.

#### A Mathematical Theory

In the remainder of this section we shall assume that we are given a finite number of samples  $\{k_0(r_i, r_j) : 1 \leq i, j \leq n\}$  of the covariance function of the zeroth-order Fourier coefficient process  $y_0(r)$  corresponding to the measurements  $y(r_i, \theta)$  of (2.15). A procedure for estimating  $k_0(r_i, r_j)$  from the given measurements will be presented in the next section. Note

that under the assumptions of Section 2 (see (2.13)-(2.17)),  $k_0(r_i, r_j)$  is of the form

$$k_0(r_i, r_j) = \sum_{l=1}^L P_l J_0(\lambda_l r_i) J_0(\lambda_l r_j) + \frac{\sigma^2}{2\pi} \frac{\delta_{i,j}}{r_i}. \quad (3.2)$$

The first step in our algorithm is to construct a symmetric matrix out of the given sample values of  $k_0(r, s)$ . Denote by  $k_{ij}$

$$k_{ij} = \sqrt{r_i r_j} k_0(r_i, r_j). \quad (3.3)$$

Note that  $k_{ij}$  is a normalized version of  $k_0(r_i, r_j)$ . The normalization is introduced here to make the measurement noise intensity constant instead of inversely proportional to  $r_i$  (see (3.2)). This will enable us to solve the cylindrical harmonics retrieval problem by performing an eigenanalysis of the normalized zeroth order covariance matrix  $R = [k_{ij}]$ . In particular, note that the matrix  $R$  can be written as

$$R = S + \frac{\sigma^2}{2\pi} I_{n \times n}, \quad (3.4)$$

where  $S$  is an  $n \times n$  symmetric matrix with entries

$$s_{ij} = \sum_{l=1}^L \sqrt{r_i r_j} P_l J_0(\lambda_l r_i) J_0(\lambda_l r_j). \quad (3.5)$$

Furthermore, it is clear from (3.5) that  $S$  can be decomposed as

$$S = CDC^T, \quad (3.6)$$

where  $D = \text{diag}\{P_l\}$  is an  $L \times L$  diagonal matrix, and where  $C$  is an  $n \times L$  matrix with entries

$$c_{ij} = \sqrt{r_i} J_0(\lambda_j r_i). \quad (3.7)$$

In the sequel, we assume that  $C$  has full column rank. Hence, the rank of  $S$  is equal to  $\min(n, L)$ . This key observation will allow us to recover both the measurement noise power  $\sigma^2$  and the cylindrical harmonics frequencies  $\lambda_l$  by performing an eigenanalysis of the matrix  $R$ .

To estimate the noise power  $\sigma^2$ , we note that if  $n > L$ , then the  $(n - L)$  smallest eigenvalues of  $R$  are exactly equal to  $\sigma^2/2\pi$ . Hence, the measurement noise power can be computed as  $2\pi\mu_{\min}$ , where  $\mu_{\min}$  is the smallest eigenvalue of  $R$ .

The location of the cylindrical harmonics can be determined by observing that if  $\mathbf{y}_m = [y_m(i)]$ ,  $1 \leq m \leq (n - L)$ , is an eigenvector of  $R$  corresponding to the repeated eigenvalue  $\sigma^2/2\pi$ , then

$$S\mathbf{y}_m = 0. \quad (3.8)$$

Equation (3.8) implies that

$$\sum_{l=1}^L P_l \sqrt{r_l} J_0(\lambda_l r_l) \sum_{j=1}^n \sqrt{r_j} J_0(\lambda_l r_j) y_m(j) = 0, \quad \forall i. \quad (3.9)$$

If we denote by  $f_m(\lambda)$  the quantity

$$f_m(\lambda) = \sum_{i=1}^n \sqrt{r_i} J_0(\lambda r_i) y_m(i), \quad (3.10)$$

then equation (3.9) is equivalent to

$$CD \begin{bmatrix} f_m(\lambda_1) \\ \vdots \\ f_m(\lambda_L) \end{bmatrix} = 0, \quad (3.11)$$

where  $CD$  has full rank, so that we must have

$$f_m(\lambda_l) = 0 \quad (3.12)$$

for  $1 \leq m \leq n - L$  and  $1 \leq l \leq L$ . Hence, the cylindrical harmonic frequencies  $\lambda_l$  appearing in (2.13) must be the roots of the equation

$$f_m(\lambda) = 0. \quad (3.13)$$

However, equation (3.13) is not useful as a practical way of computing the values of the cylindrical frequencies. The roots of (3.13) are very sensitive to perturbations in the entries of the matrix  $R$  because the coefficients of (3.13) come from a single eigenvector associated with the smallest eigenvalue of  $R$ . To avoid this problem, we can use the whole eigenspace associated with the smallest eigenvalue of  $R$ , and take our estimates of the cylindrical frequencies to be the roots of the equation

$$\sum_{m=1}^{n-L} f_m^2(\lambda) = 0. \quad (3.14)$$

Finally, to compute the amplitudes  $P_l$  of the cylindrical harmonics, we use the fact that

$$\sqrt{r_i r_j} k_0(r_i, r_j) = \sum_{l=1}^L \sqrt{r_i r_j} P_l J_0(\lambda_l r_i) J_0(\lambda_l r_j) + \frac{\sigma^2}{2\pi} \delta_{i,j}, \quad 1 \leq i, j \leq n. \quad (3.15)$$

Because of the symmetry of  $R$ , there are only  $n(n+1)/2$  identities of the form (3.15). By properly scanning the indices  $i$  and  $j$ , these  $n(n+1)/2$  identities can be written in matrix form as

$$\mathbf{k} = A\mathbf{p} \quad (3.16)$$

where the vectors  $\mathbf{k}$  and  $\mathbf{p} = [P_l]$  are of size  $\frac{n(n+1)}{2} \times 1$  and  $p \times 1$  respectively, and where  $A$  is a matrix of appropriate dimensions. The estimated cylindrical harmonics amplitudes are then taken to be equal to the entries of the optimal solution  $\mathbf{p}^*$  to (3.16), i.e. the one that minimizes the Euclidean norm of the error  $\|\mathbf{k} - A\mathbf{p}\|$ . Note that it is well known that  $\mathbf{p}^*$  is given by the equation [14]

$$\mathbf{p}^* = (A^T A)^{-1} A^T \mathbf{k}. \quad (3.17)$$

## B Numerical Implementation

The eigenvalues and eigenvectors of  $R$  can be computed numerically by first reducing the matrix  $R$  to a tridiagonal form by means of Householder transformations and then using the QR algorithm to generate the eigenvalues. The eigenvectors of  $R$  can be computed by saving and then multiplying together the transformations used in the first step. The above procedure has been implemented as part of a singular value decomposition routine available through Linpack [15] and was found to be numerically robust and highly accurate. Its only deficiency lies in its complexity; it requires  $O(n^3)$  operations where  $n$  is the size of the square symmetric matrix  $R$ .

In practice, due to inaccuracies in the estimated values of  $k_0(r_i, r_j)$ , the computed smallest eigenvalues of  $R$  are not all exactly equal, and the noise power has to be computed as the average of the  $(n-L)$  cluster of smallest eigenvalues of  $R$ . Furthermore, the separation between the “large” eigenvalues of  $R$  and the “small” eigenvalues of  $R$  is sometimes not well

marked and it is difficult to determine the exact number of harmonics in the given zeroth order Fourier coefficient covariance data. In this case statistical methods can be used to determine the number of cylindrical harmonics. (See [16] for a discussion of how statistical methods can be used to determine the number of signals in the one-dimensional case.)

The search for the cylindrical harmonics is done by plotting  $v(\lambda) = 1/\sum_{m=1}^{n-L} f_m^2(\lambda)$ , where  $f_m(\lambda)$  is defined in (3.10). The roots of equation (3.14) correspond to peaks of  $v(\lambda)$ . This step is numerically robust and poses no problems.

Finally, the estimation of the amplitudes of the cylindrical harmonics via equation (3.17) is done by performing a QR decomposition of the matrix  $A$ . The total number of operations involved in this step is of the order of  $\frac{n(n+1)}{2}L^2 - \frac{L^3}{3}$ , where  $L$  is the number of harmonics to be estimated and  $\frac{n(n+1)}{2}$  is the total number of correlations available.

## C Summary

In summary, given sample values of the covariance function  $k_0(r_i, r_j)$  corresponding to the zeroth-order Fourier coefficient process associated with the measurements  $y(\vec{r})$  of (2.15), the cylindrical harmonics retrieval problem can be solved by performing the following steps:

1. For a suitably large  $n$ , determine all of the eigenvalues and eigenvectors of the  $n \times n$  covariance matrix  $R$  obtained from the normalized sample values of the zeroth order Fourier process covariance function. The noise power is equal to  $2\pi\bar{\mu}$ , where  $\bar{\mu}$  is the average of the  $(n - L)$  cluster of smallest eigenvalues of  $R$ . The number  $L$  of larger eigenvalues is equal to the number of cylindrical harmonics.
2. Let  $f_m(\lambda)$ ,  $1 \leq m \leq n - L$ , be the functions given by (3.10) and which are specified by the eigenvectors  $y_m$  corresponding to the  $(n - L)$  smallest eigenvalues of  $R$ . Determine the roots of equation (3.14) by plotting  $v(\lambda) = 1/\sum_{m=1}^{n-L} f_m^2(\lambda)$ . The computed roots are the estimates of the values of the  $L$  cylindrical frequencies in (2.13).

3. Using equation (3.17), determine the amplitudes  $\{P_l : 1 \leq l \leq L\}$  of the  $L$  cylindrical harmonics.

The next section examines the problem of obtaining unbiased and consistent estimates of  $k_0(r_i, r_j)$  from the given field measurements.

## 4 ESTIMATION OF THE COVARIANCE FUNCTIONS

The algorithm that we presented in the last section is based on the knowledge of  $k_0(r_i, r_j)$ , the covariance function of the zeroth order-Fourier coefficient process corresponding to the measurements  $y(\vec{r})$ . However in practice, one is given the measurements themselves rather than  $k_0(r_i, r_j)$ . In this section, we present an *unbiased* and *consistent* procedure for estimating the *non-stationary* covariance function  $k_0(r_i, r_j)$  from the measurements. This procedure is well suited for the sampling geometry that we introduced in Section 2, and where the isotropic random field of interest is measured along a discrete set of concentric circles (see the discussion preceding (2.15)). Other methods for estimating  $k_0(r_i, r_j)$  from the data can be found in [17].

### A Theory

Let us start by assuming that measurements of the field  $y(\vec{r})$  are available at all the points inside the disk  $D_{R^*} = \{\vec{r} : 0 \leq r \leq R^*\}$ . Then to estimate  $k_0(r_i, r_j)$ , we can use a two step procedure. In the first step we estimate  $K(r)$  using the given data. In the second step we substitute our estimate of  $K(r)$  into (2.8) with  $n = 0$  to obtain  $k_0(r_i, r_j)$ .

$K(r)$  can be estimated by using a simple extension of the 1-D techniques that were developed to estimate the covariance function of ergodic stationary processes. Observe that along any line  $\phi = \phi_0$  in a tomographic coordinate system<sup>1</sup>,  $y(\vec{r})$  is stationary. Hence, given the measurements  $\{y(t, \phi_0) : -R^* \leq t \leq R^*\}$  along this line we can estimate  $K(r)$  using a simple extension of the 1-D techniques as

$$\hat{K}(r : \phi_0) = \frac{1}{R^{*2}} \int_{-R^*}^{R^*} y(t, \phi_0) y(r+t, \phi_0) |t| dt. \quad (4.1)$$

Since measurements of  $y(\vec{r})$  are assumed to be available all over the disk  $D_{R^*}$ , we can compute  $\hat{K}(r : \phi_0)$  for all  $\phi_0$ ,  $0 \leq \phi_0 \leq \pi$ , and take  $\hat{K}(r)$  to be

---

<sup>1</sup>A tomographic coordinate system  $(t, \phi)$  is a modified polar coordinate system where  $t$  takes both positive and negative real values, and where  $\phi$  varies from 0 to  $\pi$ .

the average of the  $\hat{K}(r : \phi_0)$  over all  $\phi_0$ . In other words, we can estimate  $K(r)$  as

$$\hat{K}(r) = \frac{1}{\pi R^{*2}} \int_0^{R^*} ds \int_0^{2\pi} d\theta s y(s, \theta) y(r + s, \theta). \quad (4.2)$$

Note that we have used the weight function  $w(t) = |t|$  in (4.1) to guarantee that  $\hat{K}(r)$  corresponds to a spatial average.

Next, we can use  $\hat{K}(r)$  to obtain an estimate of  $k_0(r_i, r_j)$  by simply substituting  $\hat{K}(r)$  for  $K(r)$  into (2.8). Thus, we take as our estimate of  $k_0(r_i, r_j)$  the quantity

$$\hat{k}_0(r_i, r_j) = \frac{1}{2\pi} \int_0^{2\pi} d\theta \hat{K}((r_i^2 + r_j^2 - 2r_i r_j \cos \theta)^{1/2}). \quad (4.3)$$

Note that according to (4.3) one needs to estimate  $K(r)$  for  $0 \leq r \leq 2r^*$  in order to be able to estimate  $k_0(r_i, r_j)$  for  $0 \leq r_i, r_j \leq r^*$ .

Let us now study the unbiasedness and consistency properties of the estimates (4.2) and (4.3). It is a simple matter to show that  $\hat{K}(r)$  is an unbiased estimate of  $K(r)$ . Equation (4.2) implies that

$$\begin{aligned} E[\hat{K}(r)] &= \frac{1}{\pi R^{*2}} \int_0^{R^*} ds \int_0^{2\pi} d\theta s K(r) \\ &= K(r), \end{aligned} \quad (4.4)$$

which proves that  $\hat{K}(r)$  is indeed an unbiased estimate of  $K(r)$ . Furthermore, it can be shown that  $\hat{K}(r)$  is a consistent estimate of  $K(r)$  under the assumption that the underlying random field is Gaussian. The proof of this fact uses a number of properties of the Bessel functions and can be found in the Appendix.

To show that  $\hat{k}_0(r_i, r_j)$  is an unbiased and consistent estimate of  $k_0(r_i, r_j)$ , we note that (2.8) and (4.3) imply that  $k_0(r_i, r_j)$  and  $\hat{k}_0(r_i, r_j)$  are related linearly to  $K(r)$  and  $\hat{K}(r)$  respectively. Hence, it follows immediately from the unbiasedness and consistency properties of  $\hat{K}(r)$  that  $\hat{k}_0(r_i, r_j)$  is an unbiased and consistent estimate of  $k_0(r_i, r_j)$ . Thus, by using (4.2) and (4.3) we are able to obtain an unbiased and consistent estimate of the non-stationary covariance function  $k_0(r_i, r_j)$ .

## B Numerical Implementation

In practice we are given the values of the field  $y(\vec{r})$  at discrete points  $\{(r_i, \theta_j) : 1 \leq i \leq I, 1 \leq j \leq J\}$ . Let us assume for simplicity that  $r_i = i\Delta$  where  $\Delta$  is a positive number, and that  $\theta_j = (j-1)2\pi/J$ . The estimate  $\hat{K}(r)$  can be computed by approximating the 2-D integral (4.2) with a rectangular rule in the radial coordinate  $s$ , and with a trapezoidal rule in the angular coordinate  $\theta$  as

$$\hat{K}(l\Delta) \approx \frac{2}{I^2 J} \sum_{i=1}^I \sum_{j=1}^J i y(i\Delta, (j-1)\frac{2\pi}{J}) y((i+l)\Delta, (j-1)\frac{2\pi}{J}). \quad (4.5)$$

The estimated covariance  $k_0(i, j)$  can then be computed by similarly approximating the integral (4.3) with a trapezoidal rule as

$$\hat{k}_0(l_1, l_2) \approx \frac{1}{J} \sum_{j=1}^J \hat{K}((l_1^2 + l_2^2 - 2l_1 l_2 \cos(j-1)\frac{2\pi}{J})^{1/2}). \quad (4.6)$$

Note that to compute  $\hat{k}_0(l_1, l_2)$  via (4.11) we may need the value of  $\hat{K}(\cdot)$  at points not equal to some multiple of  $\Delta$ . However, if  $\Delta$  is chosen small enough, we can interpolate the values of  $\hat{K}(r)$  at the required abscissas from the values of  $\hat{K}(r)$  at the points  $r = k\Delta$  using any of the known interpolation schemes. In our experiments we used a linear interpolation procedure. Better, but computationally more expensive ways of approximating the integrals in (4.2) and (4.3) can be found in [18].

## C Example

We now illustrate the behavior of our estimation procedure with an example. The example clearly indicates the fact that as more and more data is available the estimates that we get become better and better. This is to be expected since our estimators are consistent.

### Example 4.1

In this example we used the method of [19] to generate an isotropic random field with a covariance function consisting of two cylindrical harmonics at 0.1 rad/m and 0.3 rad/m. The amplitudes of both harmonics

were taken to be equal to 10 Watts. The field was generated on a circular polar grid at the points  $(0.1i, (j-1)\frac{2\pi}{50})$ . We then added to this field a 2-D white noise field of intensity 3 Watt.m<sup>2</sup>. Thus, over the rectangular grid  $r = i, s = j$  the covariance function of the zeroth-order Fourier coefficient corresponding to the resulting field has the form

$$k_0(i, j) = 10J_0(0.1i)J_0(0.1j) + 10J_0(0.3i)J_0(0.3j) + \frac{3}{2\pi i}\delta_{i,j}. \quad (4.7)$$

The corresponding power spectrum is shown in Fig. 1. Using the values of the resulting field over the disk  $0 \leq r \leq 30$ , we used (4.10) to compute  $\hat{K}(l\Delta)$  for  $\Delta = 0.1$  and for  $0 \leq l \leq 200$ , and then used these values to compute  $k_0(i, j)$  for  $1 \leq i, j \leq 10$  via (4.11). The estimated covariance function  $\hat{K}(l\Delta)$  that we computed is plotted in Fig. 2 together with the exact covariance function. Fig. 2 shows that the relative error in the estimated values of  $K(l\Delta)$  was less than 2.2 percent for  $l \leq 10$  and less than 130 percent for all  $l$ . The corresponding relative error in the estimated values of  $k_0(i, j)$  was on the average around 40 percent and was equal to 246 percent in one case. By using the values of the field over the disk  $0 \leq r \leq 100$  we obtained the estimated covariance function  $\hat{K}(l\Delta)$  that is plotted in Fig. 3. In this case, the relative error in the estimates  $\hat{K}(l\Delta)$  was less than 1.6 percent for  $l \leq 10$  and less than 70 percent for all  $l$ , while the relative error in the estimated values of  $k_0(i, j)$  was on the average around 30 percent and was still equal to 246 percent in one case. Note that as with any covariance estimation method whether in 1-D or in 2-D, one expects a degradation in performance as  $l$  increases because of the reduction in the extent of spatial averaging that can be done. This effect can clearly be seen in this example. Indeed, Fig. 1 and 2 show that the large relative errors in the values of  $\hat{K}(l\Delta)$  occur for large lags. Furthermore, by comparing Fig. 1 and 2 we observe an increase in the range of lags over which  $\hat{K}(l\Delta)$  can be estimated accurately when we expand the set of available data. The overall improvement in the accuracy of our estimates when more data is used in (4.10) is a direct result of the fact that our estimator is consistent and should not come as a surprise. Note also that the improvement in the estimates of  $k_0(i, j)$  when more data is used is relatively smaller than the corresponding improvement in the estimates of  $K(l\Delta)$  for large values of  $l$ . This seems to be due to the fact that the relative improvement in the accuracy of the

estimates of  $K(l\Delta)$  for small  $l$  is small and that these values tend to be used repeatedly in computing  $\hat{k}_0(i, j)$ . Furthermore, part of the inaccuracy of the estimated values of  $k_0(i, j)$  is due to both the approximation errors and the interpolation errors that occur in the process of computing  $\hat{k}_0(i, j)$  via equation (4.11). However, as we shall see in the next section, the inaccuracy of the estimated values of  $k_0(i, j)$  does not seriously affect the performance of our cylindrical harmonics retrieval algorithm.

## 5 EXAMPLES

The objective of this section is to illustrate some properties of the algorithm of Section 3 with two examples. The first example uses the synthetic data generated for Example 4.1 while the second example uses exact covariance values. Example 5.1 clearly displays the robustness of our procedure and its high resolution properties, even when relatively inaccurate estimates of  $k_0(i, j)$  are used as an input to our method. Example 5.2 is meant to show the robustness of our algorithm in the presence of modeling errors.

### Example 5.1

In this example we consider the data generated for Example 4.1 and use the resulting estimates of  $k_0(i, j)$  as an input to our procedure. Recall that the exact form of  $k_0(i, j)$  for the data of Example 4.1 is

$$k_0(i, j) = 10J_0(0.1i)J_0(0.1j) + 10J_0(0.3i)J_0(0.3j) + \frac{3}{2\pi i}\delta_{i,j}, \quad (5.1)$$

Recall also that this corresponds to a signal with a power spectrum consisting of two cylindrical impulses at 0.1 rad/m and 0.3 rad/m respectively, and which have both an amplitude of 10 watts, i.e. the power spectrum of the signal is of the form

$$S(\lambda) = 10\frac{\delta(\lambda - 0.1)}{\lambda} + 10\frac{\delta(\lambda - 0.3)}{\lambda}. \quad (5.2)$$

Observe that the noise intensity in the data of Example 4.1 is 3 watts.m<sup>2</sup>. Thus, the total noise power in the wave-number band [0,1] rad/m is only 0.25 dB lower than that of either cylindrical impulse. The exact power spectrum of the observations (i.e. of the signal plus noise field) is shown in Fig. 1.

When we used the estimates of  $k_0(i, j)$ ,  $1 \leq i, j \leq 10$ , which were computed in Example 4.1 from the data inside the disk  $0 \leq r \leq 30$ , we obtained the results shown in Table 1 and Fig. 4. Table 1 lists the eigenvalues of  $R$ . It is clear from this list that two eigenvalues are considerably

larger than the other ones and must therefore be associated with cylindrical harmonics. However, there exists several intermediate eigenvalues which might correspond to low energy harmonics. To determine whether this is the case, we plot in Fig. 4 the function  $v(\lambda)$  formed with the eigenvectors of  $R$  corresponding to its five smallest eigenvalues. Note that this means that our initial guess for the number of cylindrical harmonics is five. From Fig. 4 we see that  $v(\lambda)$  has only two peaks corresponding to the presence of cylindrical harmonics at 0.134 rad/m and 0.285 rad/m, so that the intermediate eigenvalues of  $R$  do not correspond to low level harmonics. These intermediate eigenvalues can be attributed to the fact that we have used noisy estimates of the covariance  $k_0(i, j)$  as an input to our algorithm. The five smallest eigenvalues of  $R$  correspond to an estimated noise intensity of 2.50 watt.m<sup>2</sup>. Finally, the amplitudes of the cylindrical harmonics were computed via (3.17) to be 10.29 and 9.69 watts respectively. Hence, the estimated signal power spectrum is

$$S(\lambda) = 10.29 \frac{\delta(\lambda - 0.134)}{\lambda} + 9.69 \frac{\delta(\lambda - 0.285)}{\lambda}. \quad (5.3)$$

Note that our algorithm is quite robust since it performed well even though the relative error in the estimated values of  $k_0(i, j)$  is relatively large, as was noted in our discussion of Example 4.1.

When we used the estimates of  $k_0(i, j)$ ,  $1 \leq i, j \leq 10$ , which were computed in Example 4.1 from the data inside the disk  $0 \leq r \leq 100$ , we obtained the results shown in Table 2 and Fig. 5. Table 2 lists the eigenvalues of  $R$  and Fig. 5 is a plot of  $v(\lambda)$ . In this case, the estimated signal power spectrum that we find is given by

$$S(\lambda) = 9.62 \frac{\delta(\lambda - 0.096)}{\lambda} + 10.35 \frac{\delta(\lambda - 0.298)}{\lambda}. \quad (5.4)$$

The estimated noise strength using the values of the four smallest eigenvalues of  $R$  (see Table 2) is 2.98 watt.m<sup>2</sup>. Note the improvement in the estimates in general, and particularly in the location of the cylindrical frequencies. This improvement is a direct result of the fact that we have used more accurate estimates of  $k_0(i, j)$  as an input to our algorithm. In fact, the performance of our algorithm is limited only by the accuracy of the

estimated values of  $k_0(i, j)$ . With the exact values of  $k_0(i, j)$ ,  $1 \leq i, j \leq 10$ , used as an input to our procedure, the computed eigenvalues of  $R$  and a scaled-down version of the corresponding  $v(\lambda)$  formed with the eigenvectors corresponding to the five smallest eigenvalues of  $R$ , are shown in Table 3 and Fig. 6 respectively. In this case the estimated noise intensity is 3 watt.m<sup>2</sup> and the estimated signal power spectrum is exactly equal to the actual signal power spectrum.

Finally, to demonstrate the high resolution property of our algorithm, we used a conventional spectral estimation method on the estimated values of the field covariance function  $K(r)$  that were computed in Example 4.1 using the data inside the disk  $0 \leq r \leq 100$ . The conventional power spectral estimate was taken to be equal to a weighted Hankel transform of the estimated field covariance function  $K(r)$  [2]. The weighting function that we chose was of the form

$$w(r) = \begin{cases} 2 \cos^{-1} \frac{r}{20} - \frac{r}{10} \sqrt{1 - (\frac{r}{20})^2} & 0 \leq r \leq 20, \\ 0 & \text{otherwise.} \end{cases} \quad (5.5)$$

The Hankel transform of this weighting function is

$$2\pi \frac{J_1^2(10\lambda)}{\lambda^2}, \quad (5.6)$$

and is positive for all frequencies. Hence, the expected value of the conventional power spectral estimate obtained by using this window is guaranteed to be positive [2]. The computed estimate is shown in Fig. 7. Note that the conventional method does not resolve the two cylindrical harmonics. This should not come as a surprise since the resolution of conventional spectral estimation is always inversely proportional to the spatial extent of the interval over which  $K(r)$ , or its estimate, is given, *regardless* of the choice of the window [2]. In our case an estimate of  $K(r)$  was computed over the interval  $[0, 20]$ . This implies that the resolution of any conventional spectral estimation method is on the order of 0.3 radians/m, which is much larger than the separation between the cylindrical harmonics of (5.2).

### Example 5.2

In this example we demonstrate the robustness of our algorithm with respect to modeling errors. Since we have already analyzed the effect of

errors due to inaccurate covariance estimates in Example 5.1, we shall use exact covariance data in order to focus our attention on errors due to inaccuracies in the signal power spectrum model.

Consider a signal power spectrum of the form

$$S(\lambda) = 10 \frac{\delta(\lambda - 0.1)}{\lambda} + 15 \frac{\delta(\lambda - 0.2)}{\lambda} + 10 \frac{\delta(\lambda - 0.3)}{\lambda} + 100(u(\lambda - 0.4) - u(\lambda - 0.3)), \quad (5.7)$$

where  $u(\lambda)$  is a unit step function. Note the presence in (5.7) of a relatively strong unmodeled colored noise component whose total power is only 1.76 dB lower than that of the strongest cylindrical harmonic. The measurement noise power  $\sigma^2$  is taken to be 1 watt.m<sup>2</sup> corresponding to a total white noise power in the wave-number band [0,1] rad/m which is only 6.7 dB lower than the power of the strongest harmonic. Let us further assume that we are given exact values of  $k_0(i, j)$  for  $1 \leq i, j \leq 10$ . The computed eigenvalues of the  $10 \times 10$  symmetric matrix  $R = [\sqrt{ij}k_0(i, j)]$  are listed in Table 4. Examination of these eigenvalues reveals the presence of four cylindrical harmonics, a fact that is confirmed by the scaled-down plot of the  $v(\lambda)$  (Fig. 8) which is formed with the eigenvectors corresponding to the two smallest eigenvalues of  $R$ . In this example, the estimated measurement noise power is 1 watt.m<sup>2</sup> and the reconstructed signal power spectrum is found to be of the form

$$S(\lambda) = 10.95 \frac{\delta(\lambda - 0.104)}{\lambda} + 15.1976 \frac{\delta(\lambda - 0.208)}{\lambda} + 10.95 \frac{\delta(\lambda - 0.31)}{\lambda} + 1.39 \frac{\delta(\lambda - 0.387)}{\lambda}. \quad (5.8)$$

Note that the presence of a strong unmodeled colored noise component in the signal power spectrum has introduced a small bias in the estimated positions of the cylindrical harmonics, and has led to estimated cylindrical harmonics amplitudes which are slightly higher than their true values. Note also the presence of a spurious cylindrical harmonic at 0.387 radians/m in the reconstructed power spectrum given by (5.8). This spurious cylindrical harmonic is solely due to the unmodeled colored noise component. The fact that the unmodeled colored noise component gives rise to a spurious

cylindrical harmonic is reminiscent of what happens in the 1-D case, since it was observed in [20] that 1-D harmonic retrieval methods which are based on an eigenanalysis of the covariance matrix do produce spurious 1-D harmonics in the presence of an unmodeled colored noise component.

The above two examples, and others, show that, overall, our algorithm is quite robust, that it has a strong resolution property and that its accuracy is really limited only by the accuracy of the estimated values of  $k_0(i, j)$ .

## 6 CONCLUSION

In this paper, we have presented a high resolution spectral estimation method for isotropic random fields with a covariance function equal to a weighted sum of cylindrical harmonics. Such fields are often used to model some types of background noise in geophysics and in ocean acoustics. The algorithm that we have obtained takes maximal advantage of the symmetries implied by the special structure of covariance functions which are equal to a weighted sum of cylindrical harmonics. Our approach is similar in spirit to the 1-D spectral estimation methods based on harmonic retrieval from an eigenanalysis of the covariance matrix. In the 2-D isotropic context, the spectral estimate is determined by performing an eigenanalysis of the covariance matrix of samples of the zeroth-order Fourier coefficient process corresponding to the given noisy observations of the underlying field. We have also discussed the estimation of this covariance matrix and presented examples to illustrate the high resolution and robustness properties of our procedure.

## APPENDIX

*Proof of the consistency of  $\hat{K}(r)$ .*

The variance of the estimator  $\hat{K}(r)$  of (4.2) is given by

$$\begin{aligned} \text{var}(\hat{K}(r)) = \frac{1}{(\pi R^{*2})^2} \int_{D_{R^*}} d\vec{s}_1 \int_{D_{R^*}} d\vec{s}_2 & E[y(s_1, \theta_1)y(r + s_1, \theta_1) \\ & y(s_2, \theta_2)y(r + s_2, \theta_2)] - K^2(r). \end{aligned} \quad (\text{A.1})$$

In (A.1)  $d\vec{s}_i$  denotes the infinitesimal unit of area  $d\vec{s}_i = s_i ds_i d\theta_i$  and  $D_{R^*}$  is the disk of radius  $R^*$  centered at the origin, so that  $D_{R^*} = \{\vec{r} : r \leq R^*\}$ . Using the moment factoring property of jointly Gaussian random variables, we obtain from (A.1)

$$\begin{aligned} \text{var}(\hat{K}(r)) = \frac{1}{(\pi R^{*2})^2} \int_{D_{R^*}} d\vec{s}_1 \int_{D_{R^*}} d\vec{s}_2 & \{K((s_1^2 + s_2^2 - 2s_1s_2 \cos(\theta_1 - \theta_2))^{1/2}) \\ & \cdot K(((r + s_1)^2 + (r + s_2)^2 - 2(r + s_1)(r + s_2) \cos(\theta_1 - \theta_2))^{1/2}) \\ & + K((s_1^2 + (r + s_2)^2 - 2s_1(r + s_2) \cos(\theta_1 - \theta_2))^{1/2}) \\ & \cdot K(((r + s_1)^2 + s_2^2 - 2(r + s_1)s_2 \cos(\theta_1 - \theta_2))^{1/2})\}. \end{aligned} \quad (\text{A.2})$$

Substituting the identity [11]

$$K((s_1^2 + s_2^2 - 2s_1s_2 \cos(\theta_1 - \theta_2))^{1/2}) = \sum_{n=-\infty}^{\infty} k_n(s_1, s_2) e^{-jn(\theta_1 - \theta_2)} \quad (\text{A.3})$$

into (A.2) yields

$$\text{var}(\hat{K}(r)) = \sum_{n=-\infty}^{\infty} c_n(r, R^*), \quad (\text{A.4})$$

where

$$\begin{aligned} c_n(r, R^*) = \frac{4}{R^{*4}} \int_0^{R^*} ds_1 \int_0^{R^*} ds_2 s_1 s_2 & \{k_n(s_1, s_2)k_n(r + s_1, r + s_2) \\ & + k_n(s_1, r + s_2)k_n(r + s_1, s_2)\}, \end{aligned} \quad (\text{A.5})$$

and where we have used the fact that the series in (A.3) is uniformly convergent to interchange the orders of summation and integration [21]. To investigate the behavior of  $c_n(r, R^*)$  as  $R^*$  tends to infinity, let us substitute (2.6) into (A.5) to obtain

$$c_n(r, R^*) = \int_0^\infty d\lambda_1 \int_0^\infty d\lambda_2 \quad S(\lambda_1) S(\lambda_2) \{d_n^2(\lambda_1, \lambda_2; r, R^*) \\ + d_n(\lambda_1, \lambda_2; r, R^*) d_n(\lambda_2, \lambda_1; r, R^*)\} \quad (\text{A.6})$$

where

$$d_n(\lambda_1, \lambda_2; r, R^*) = \frac{2}{R^{*2}} \int_0^{R^*} ds_1 s_1 J_n(\lambda_1 s_1) J_n(\lambda_2 (s_1 + r)). \quad (\text{A.7})$$

We now invoke the Bessel addition theorem [11]

$$J_n(\lambda(r+s)) = \sum_{k=-\infty}^{\infty} J_{n-k}(\lambda r) J_k(\lambda s) \quad (\text{A.8})$$

and use the fact that (A.8) is a uniformly convergent series to rewrite (A.7) as

$$d_n(\lambda_1, \lambda_2; r, R^*) = \sum_{k=-\infty}^{\infty} J_{n-k}(\lambda_2 r) e_{n,k}(\lambda_1, \lambda_2; R^*), \quad (\text{A.9})$$

where the series (A.9) is also uniformly convergent, and where

$$e_{n,k}(\lambda_1, \lambda_2; R^*) = \frac{2}{R^{*2}} \int_0^{R^*} ds_1 s_1 J_n(\lambda_1 s_1) J_k(\lambda_2 s_1). \quad (\text{A.10})$$

As  $R^*$  tends to infinity and for any  $\lambda_1 \geq 0$  and any  $\lambda_2 \geq 0$ , there exist a constant  $R^{**} < R^*$  such that

$$|J_n(\lambda_1 s_1) J_k(\lambda_2 s_1)| < \frac{2}{\pi s_1 \sqrt{\lambda_1 \lambda_2}} \quad \forall s_1 > R^{**}. \quad (\text{A.11})$$

Furthermore, we have

$$\lim_{R^* \rightarrow \infty} e_{n,k}(\lambda_1, \lambda_2; R^*) = \lim_{R^* \rightarrow \infty} \frac{2}{R^{*2}} \int_0^{R^{**}} ds_1 s_1 J_n(\lambda_1 s_1) J_k(\lambda_2 s_1) \\ + \lim_{R^* \rightarrow \infty} \frac{2}{R^{*2}} \int_{R^{**}}^{R^*} ds_1 s_1 J_n(\lambda_1 s_1) J_k(\lambda_2 s_1). \quad (\text{A.12})$$

But

$$\left| \int_0^{R^{**}} ds_1 s_1 J_n(\lambda_1 s_1) J_k(\lambda_2 s_1) \right| \leq R^{**2} \quad (\text{A.13})$$

since

$$|J_n(\lambda_i s_1)| \leq 1 \quad \forall s_1 \geq 0 \text{ and } \forall \lambda_i \geq 0, \quad (\text{A.14})$$

and (A.11) implies that

$$\left| \int_{R^{**}}^{R^*} ds_1 s_1 J_n(\lambda_1 s_1) J_k(\lambda_2 s_1) \right| < \frac{2(R^{**} - R^*)}{\pi \sqrt{\lambda_1 \lambda_2}}. \quad (\text{A.15})$$

Hence

$$\lim_{R^* \rightarrow \infty} e_{n,k}(\lambda_1, \lambda_2; R^*) = 0, \quad \forall \lambda_1, \lambda_2 \geq 0, \quad (\text{A.16})$$

and since (A.9) is uniformly convergent, this means that

$$\lim_{R^* \rightarrow \infty} d_n(\lambda_1, \lambda_2; r, R^*) = 0 \quad \forall \lambda_1, \lambda_2 \geq 0 \text{ and } \forall r \geq 0. \quad (\text{A.17})$$

If we now assume that  $K(0) < \infty$  and if we use the Lebesgue dominated convergence theorem to interchange limit and integration [21], we obtain from (A.6) and (A.17)

$$\lim_{R^* \rightarrow \infty} c_n(r, R^*) = 0. \quad (\text{A.18})$$

Finally, the above equation and the fact that the series (A.4) is uniformly convergent imply that

$$\lim_{R^* \rightarrow \infty} \text{var}(\hat{K}(r)) = 0 \quad (\text{A.19})$$

which is the desired result.

## REFERENCES

- [1] J. Capon, "Maximum-Likelihood Spectral Estimation," in *Nonlinear Methods of Spectral Analysis*, S. Haykin, Ed., Springer-Verlag, New York, N.Y. 1979.
- [2] J. H. McClellan, "Multidimensional Spectral Estimation," *Proc. IEEE*, Vol. 70, No. 9, pp. 1029-1039, Sept. 1982.
- [3] R. N. McDonough, "Applications of the Maximum-Likelihood Method and the Maximum-Entropy Method to Array Processing," in *Nonlinear Methods of Spectral Analysis*, S. Haykin, Ed., Springer-Verlag, New York, N.Y. 1979.
- [4] A. B. Baggeroer, *Space/Time Random Processes and Optimum Array Processing*, Naval Undersea report NUC TP 506, San Diego, CA 1976.
- [5] S. W. Lang and J. H. McClellan, "The Extension Of Pisarenko's Method to Multiple Dimensions," in *Proc. ICASSP 82*, Paris, France, May 1982.
- [6] M. Wax and T. Kailath, "Covariance Eigenstructure Approach to 2-D Harmonic Retrieval," in *Proc. ICASSP 83*, Boston, MA, April 1983.
- [7] V. F. Pisarenko, "The Retrieval of Harmonics from a Covariance Function," *Geophys. J. Roy. Astron. Soc.*, Vol. 33, pp. 347-366, 1973.
- [8] R. O. Schmidt, "Multiple Emitter Location and Signal Parameter Estimation," in *Proc. RADC Spectrum Estimation Workshop*, Griffths AFB, N.Y., pp. 243-258, Oct. 1979.
- [9] G. Bienvenu and L. Kopp, "Adaptivity to Background Noise Spatial Coherence for High Resolution Passive Methods," in *Proc. ICASSP 80*, Denver, CO, pp. 307-310, 1980.

- [10] M. I. Yadrenko, *Spectral Theory of Random Fields*, Optimization Software Inc., New York, N.Y. 1986.
- [11] H. Bateman, *Higher Transcendental Functions*, Volume II, McGraw-Hill, New-York, N.Y. 1953.
- [12] A. Papoulis, *Systems and Transforms with Applications in Optics*, McGraw-Hill, New York, N.Y. 1968.
- [13] J. H. Wilkinson, *The Algebraic Eigenvalue Problem*, Clarendon Press, Oxford, U.K., 1965.
- [14] G. Strang, *Linear Algebra and its Applications*, Academic Press, New York, N.Y., 1980.
- [15] J. J. Dongarra et al., *Linpack User's Guide*, SIAM, Philadelphia, PA., 1979.
- [16] M. Wax and T. Kailath, "Determining the Number of Signals by Information Theoretic Criteria," in *Proc. ICASSP 84*, San Diego, California, March 1984.
- [17] A. H. Tewfik, *Recursive Estimation and Spectral Estimation for 2-D Isotropic Random Fields*, Sc.D. thesis, in preparation.
- [18] P. J. Davis and P. Rabinowitz, *Methods of Numerical Integration*, Academic Press, Orlando, FL. 1984.
- [19] M. Shinozuka and C.-M. Jan, "Digital Simulation of Random Processes and its Applications," *J. Sound Vib.*, Vol. 25, No. 1, pp. 111-128, 1972.
- [20] S. M. Kay and S. L. Marple, "Spectrum Analysis: A Modern Perspective," *Proc. IEEE.*, Vol. 69, No. 11, pp. 1380-1419, Nov. 1981.
- [21] W. Rudin, *Real and Complex Analysis*, McGraw-Hill, New York, N.Y. 1974.

## TABLE CAPTIONS

**Table 1** Eigenvalues of  $R$  in Example 5.1 when  $\hat{k}_0(i, j)$  is computed from data inside the disk  $0 \leq r \leq 30$ .

**Table 2** Eigenvalues of  $R$  in Example 5.1 when  $\hat{k}_0(i, j)$  is computed from data inside the disk  $0 \leq r \leq 100$ .

**Table 3** Eigenvalues of  $R$  in Example 5.1 when the exact values of  $k_0(i, j)$  are used.

**Table 4** Eigenvalues of  $R$  in Example 5.2.

395.6348871  
48.78233281  
1.953576725  
1.329499295  
0.963524627  
0.655533921  
0.476865723  
0.444997037  
0.245708484  
0.168982806

Table 1

470.6285589  
73.75886486  
1.966603612  
1.321482724  
1.079630800  
0.825874114  
0.717595417  
0.545082122  
0.416322808  
0.217525026

Table 2

446.8880110  
66.36065499  
0.477464780  
0.477464780  
0.477464780  
0.477464780  
0.477464780  
0.477464780  
0.477464780  
0.477464780  
0.477464780

Table 3

732.4243282  
99.73272777  
0.827748745  
0.160029111  
0.159159233  
0.159155971  
0.159154672  
0.159154011  
0.159153889  
0.159151870

Table 4

## FIGURE CAPTIONS

- Fig. 1** True spectrum  $S(\lambda)$  for Examples 4.1 and 5.1.
- Fig. 2** Plot of exact and estimated covariance functions for Example 4.1 when the estimated covariance  $\hat{K}(r)$  is computed from data inside the disk  $0 \leq r \leq 30$ .
- Fig. 3** Plot of exact and estimated covariance functions for Example 4.1 when the estimated covariance  $\hat{K}(r)$  is computed from data inside the disk  $0 \leq r \leq 100$ .
- Fig. 4** Plot of  $v(\lambda)$  for Example 5.1 when  $\hat{k}_0(i, j)$  is computed from data inside the disk  $0 \leq r \leq 30$ .
- Fig. 5** Plot of  $v(\lambda)$  for Example 5.1 when  $\hat{k}_0(i, j)$  is computed from data inside the disk  $0 \leq r \leq 100$ .
- Fig. 6** Plot of  $v(\lambda)$  for Example 5.1 when the exact values of  $k_0(i, j)$  are used.
- Fig. 7** Plot of the conventional power spectral estimate of Example 5.1.
- Fig. 8** Plot of  $v(\lambda)$  for Example 5.2.

# *Power Spectrum*

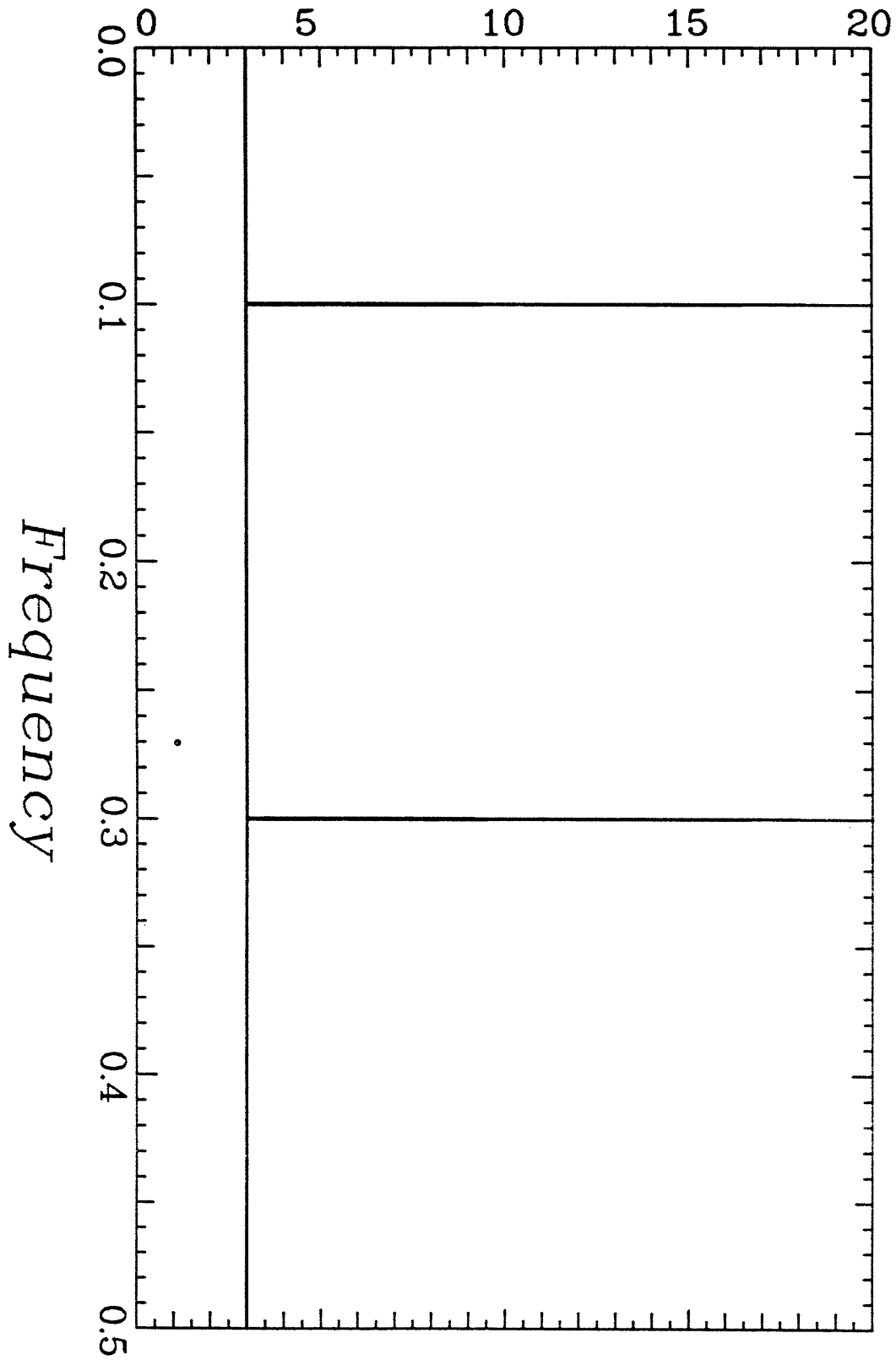


Fig. 1

# covariance

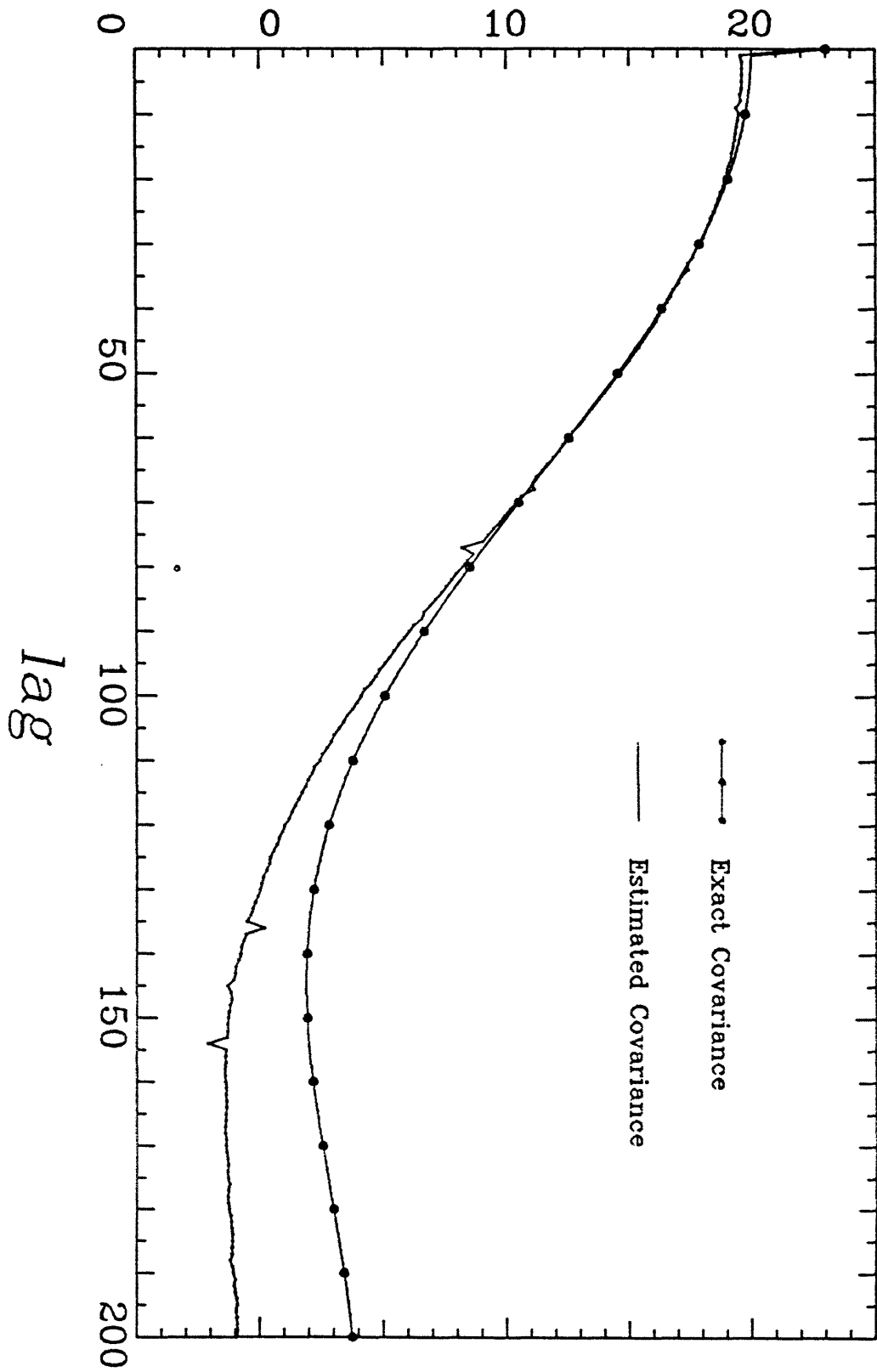


Fig. 2

# covariance

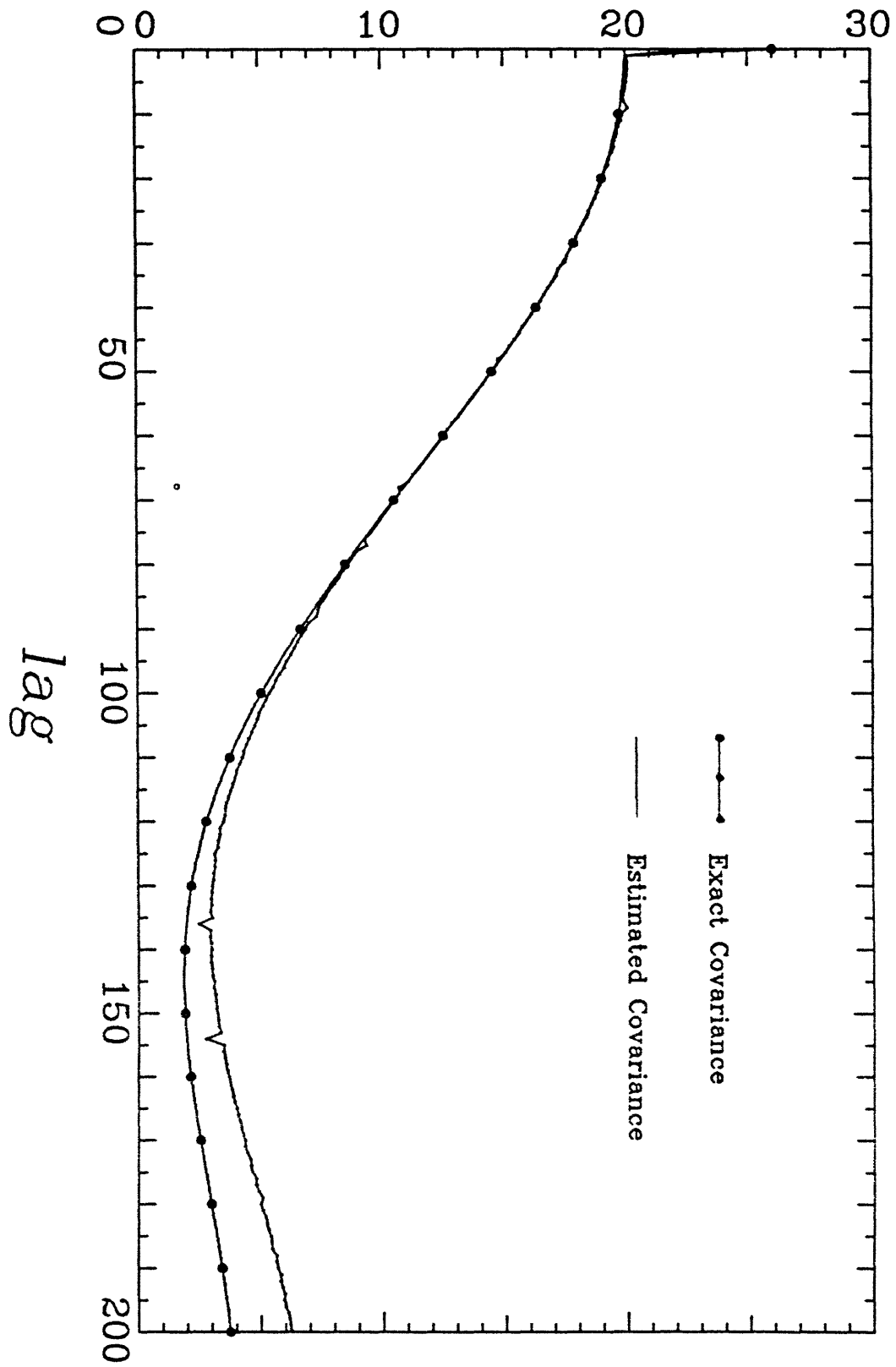


Fig. 3

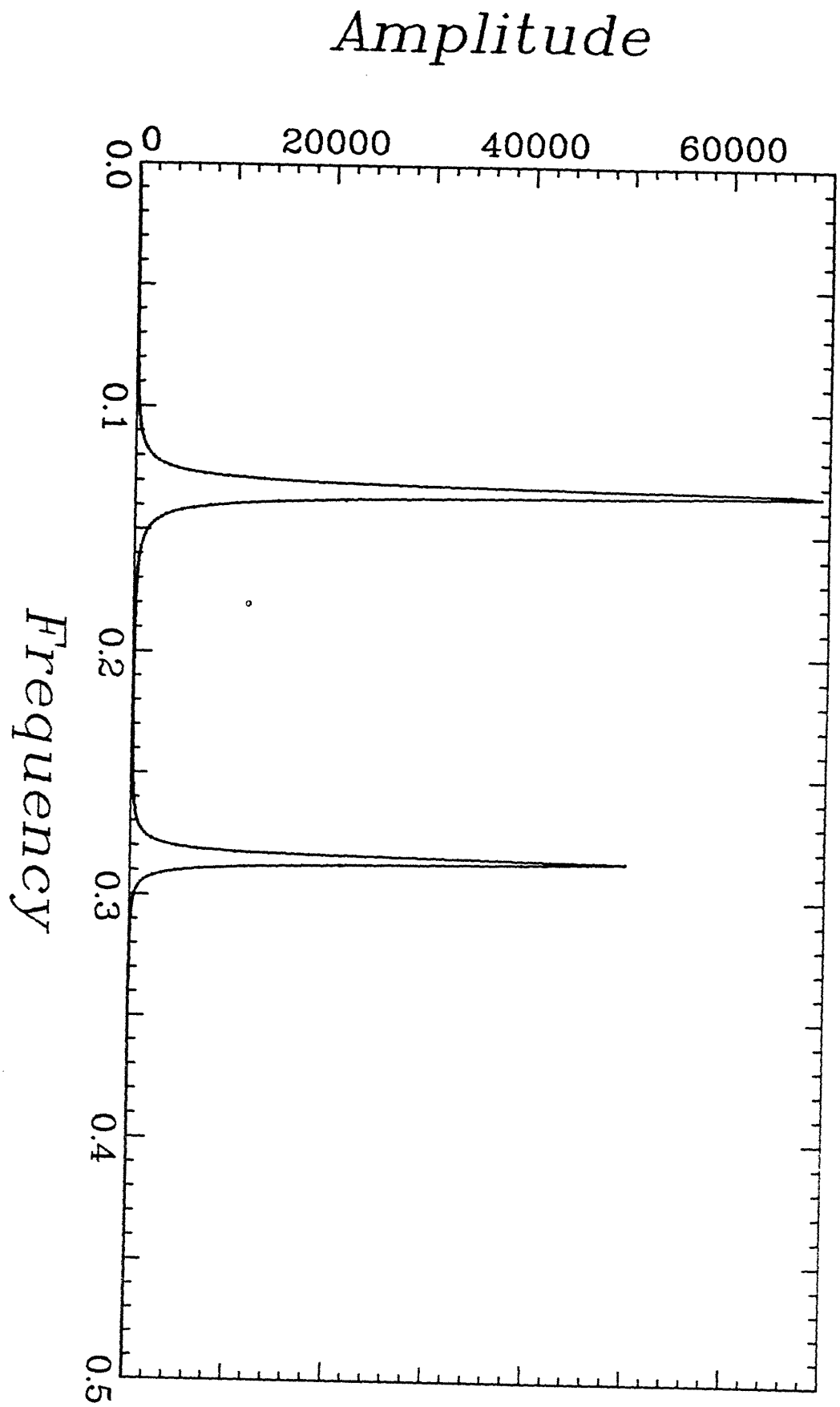


Fig. 4

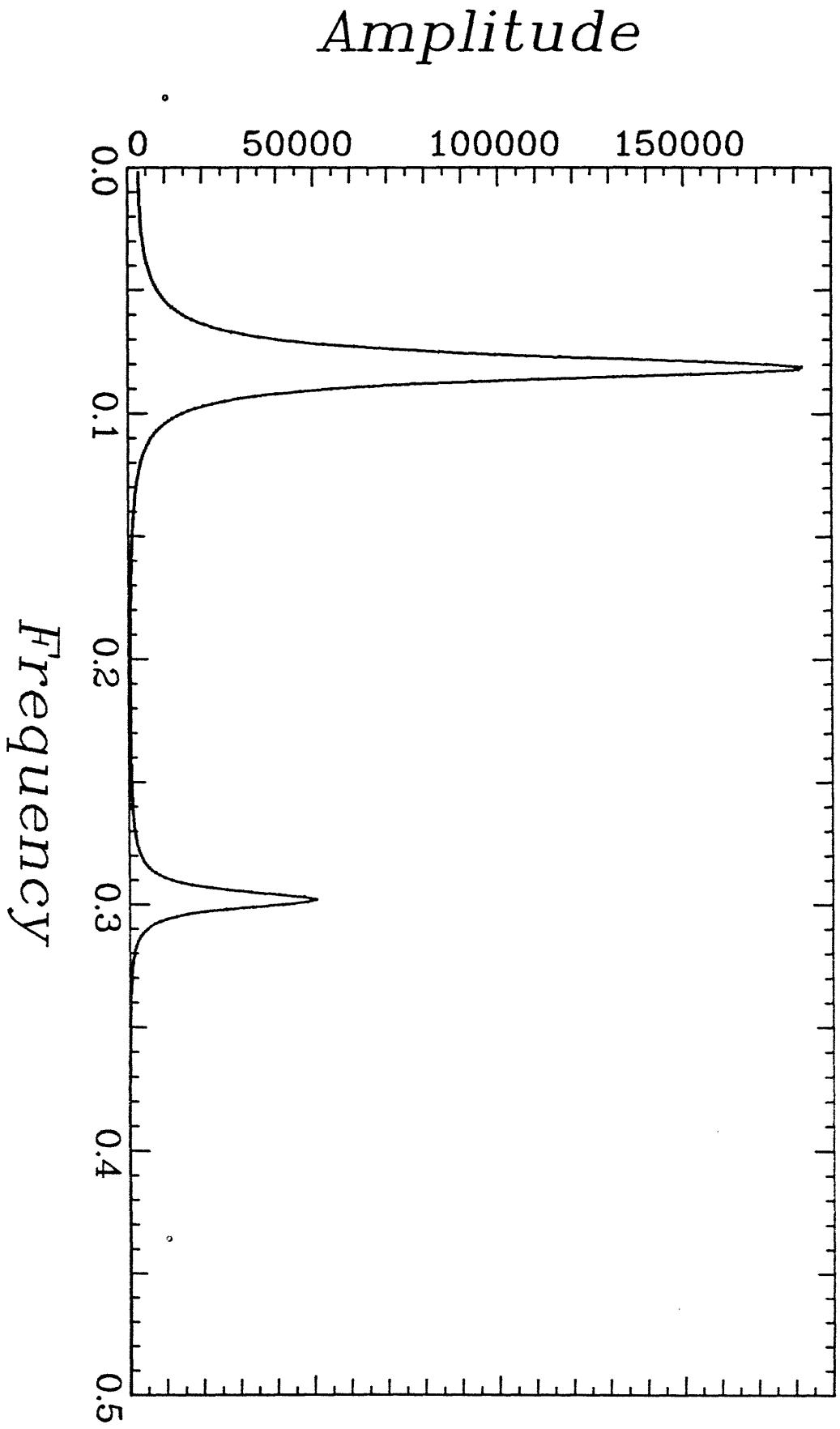


Fig. 5

*Amplitude\*10.E-23*

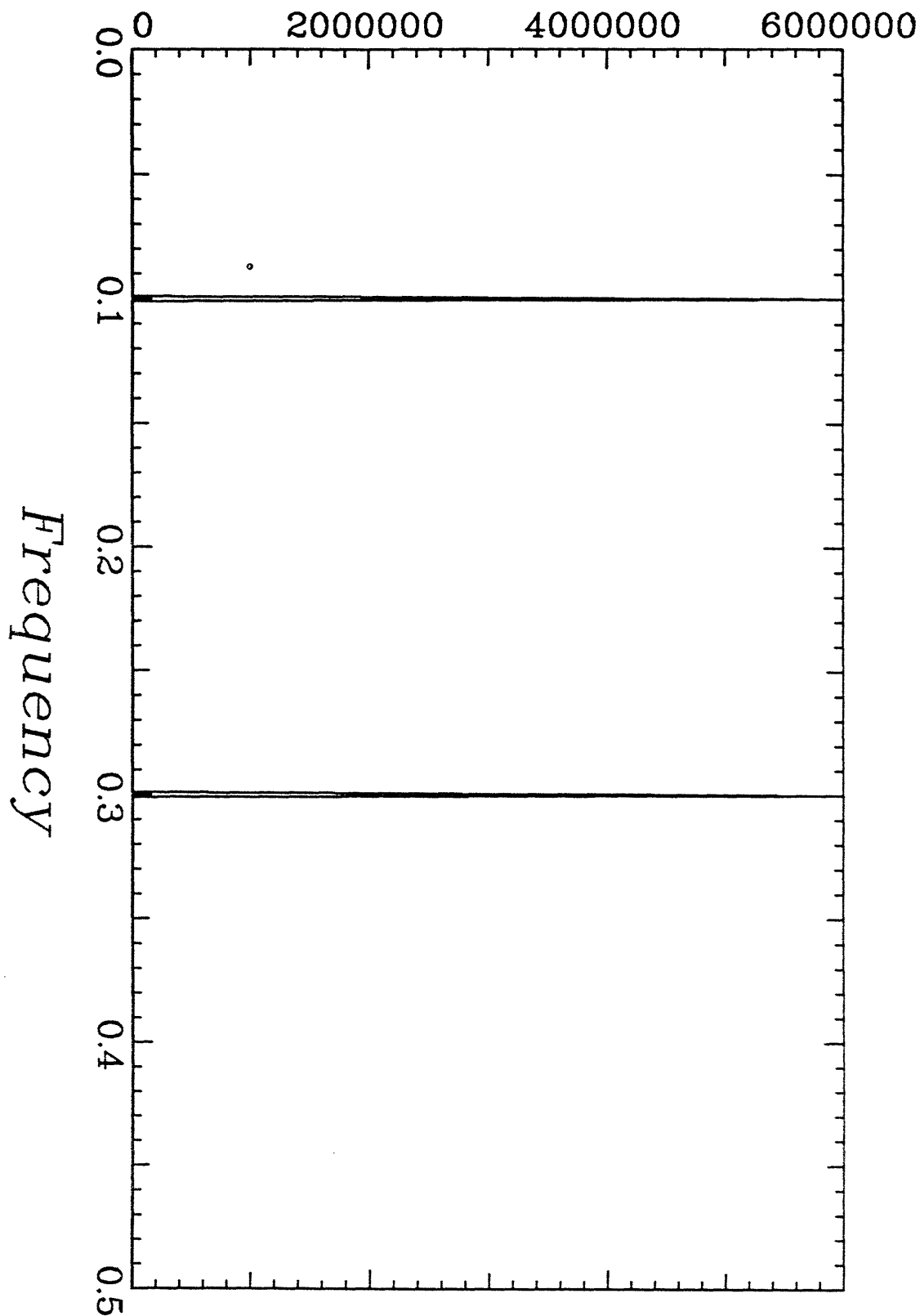


Fig. 6

# *Amplitude*

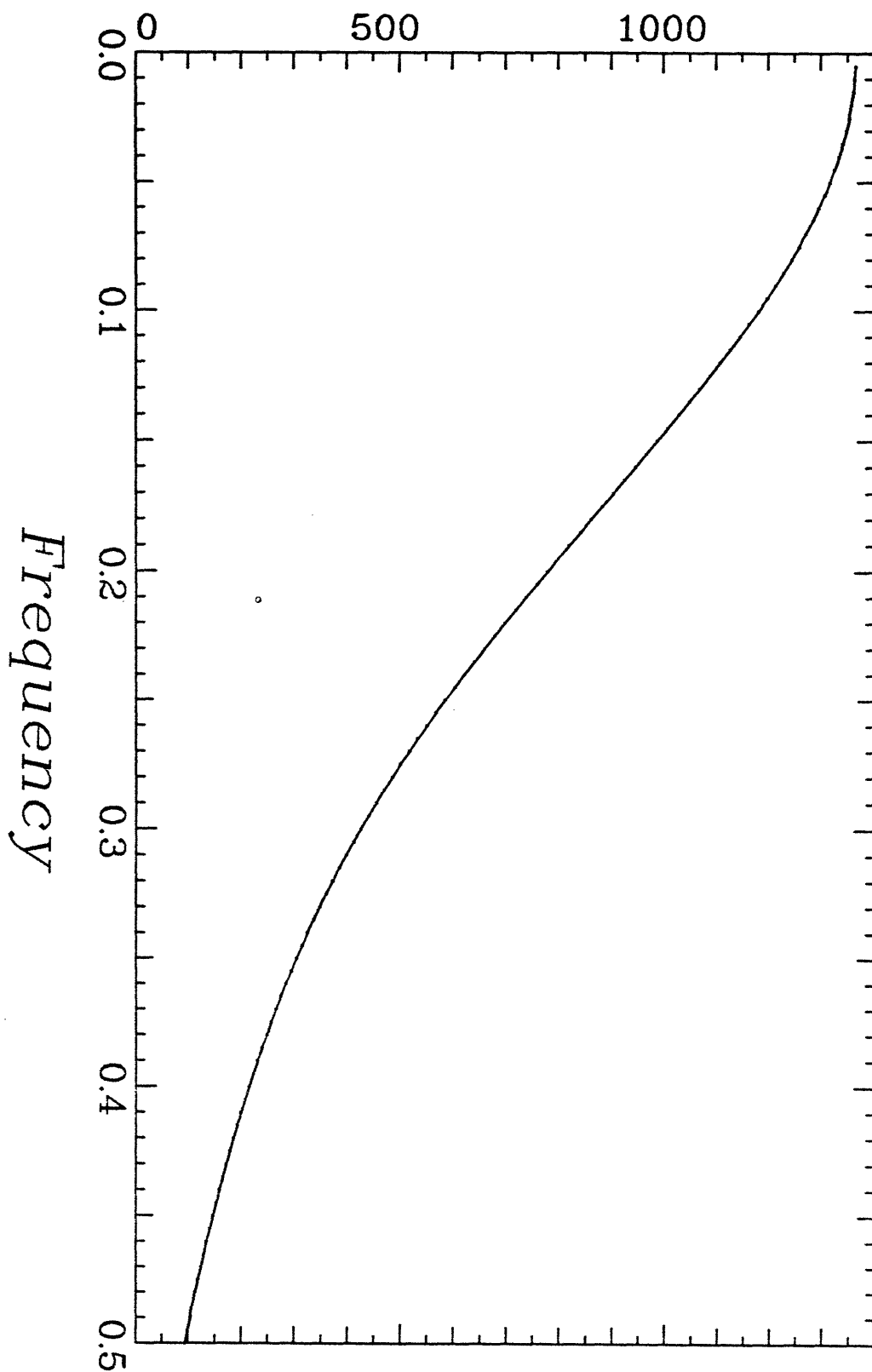


Fig. 7

*Amplitude\*1.E-9*

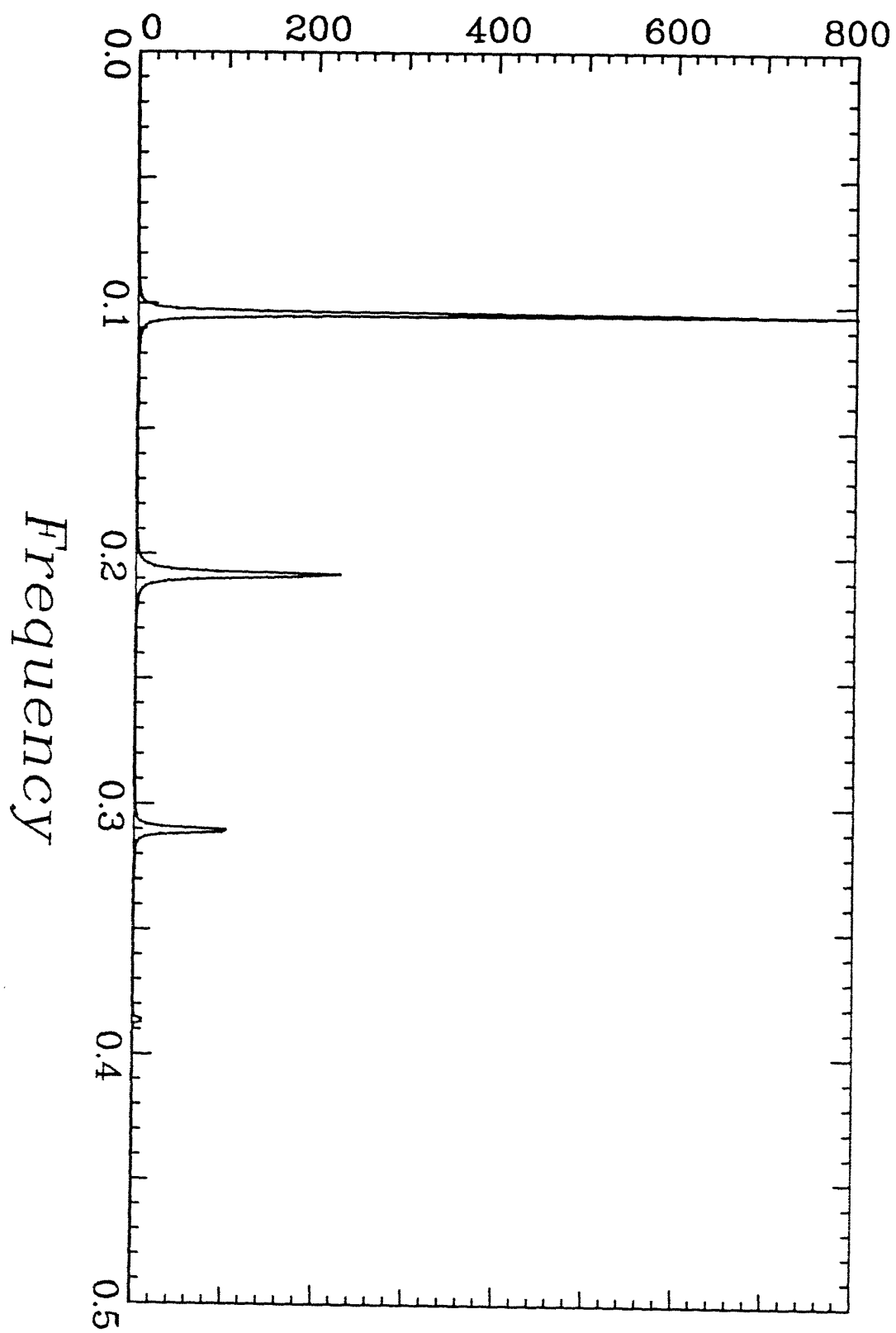


Fig. 8